Neutron-Scattering Study of Soft Modes in Cubic BaTiO₃ [†]

J. Harada, [*] J. D. Axe, and G. Shirane

Brookhaven National Laboratory, Upton, New York 11973

(Received 3 December 1970)

The soft optic phonons in the cubic phase of BaTiO₃ have been reinvestigated by the neutron-scattering technique. Measurements were carried out on major symmetry directions for a temperature range between 150 to 450 °C. It is shown that, as in the case of the tetragonal phase, the lowest transverse-optic branches along the [111] direction and one of the branches along [110] rise rapidly with increasing wave vector $\vec{q}$. Phonons are well defined except for those at very small $\vec{q}$. On the other hand, in one of the branches along [110] and in the degenerate branches along [100] the phonons are overdamped as previously shown by Yamada *et al.* for small $\vec{q}$ values. The present study extends the measurement to the entire zone and corrects the erroneous picture previously given. The most important result of the present study concerns the interaction between the soft optic modes and acoustic modes. Unusual scattering cross sections for both optic and acoustic modes are explained by interference effects in a coupled phonon model with a highly damped optic component. The interference permits, for the first time, a determination of the phase as well as the amplitude of the dynamical structure factors of the phonons involved. The energy of the optically inactive Γ_{25} mode at the Brillouin zone center was found to be (39 ± 2) meV.

I. INTRODUCTION

Neutron-scattering studies of soft ferroelectric modes in BaTiO₃ have been reported in a series of experimental work[1-3] carried out at the Brookhaven High Flux Beam Reactor. In sharp contrast to the well-behaved and clearly demonstrated soft modes[4,5] in SrTiO₃ and KTaO₃, the soft mode in the prototype ferroelectric BaTiO₃ poses a much more difficult and challenging problem. Although this is due, in part, to a difficulty in obtaining large high-quality single crystals of BaTiO₃ for inelastic neutron-scattering experiments, the basic difficulties stem from the nature of the soft mode in BaTiO₃, which has produced many conflicting results and models in the literature from the measurements using infrared,[6-8] Raman,[9-11] and x-ray[12,13] techniques.

The most recent neutron-scattering study[3] of the tetragonal phase sheds light on some basic problems. The soft optic branch shows strongly directional properties. When the polarization vector $\vec{e}$ is along [100], the soft optic mode has low energy and high damping. For other polarization vectors, the optic-mode energy rises steeply with increasing wave vector $\vec{q}$ and the relative damping decreases rapidly resulting in a well-defined phonon profile.

In the present paper, the earlier studies of cubic[1,2] BaTiO₃ are extended, with special emphasis given to the elucidation of the nature of the strong diffuse scattering which is observed in x-ray investigations.[12,13] As in the tetragonal phase,[3] the unusually strong localization of this scattering in reciprocal space is shown to result from pronounced anisotropy in the soft optic-phonon dispersion surface. An anharmonic interference between TA and TO modes is also identified and through

this understanding accurate estimates of the fundamental parameters characterizing the ferroelectric mode instability are obtained.

II. EXPERIMENTAL

The single crystal used in this study is the same crystal used previously by Yamada *et al.*[2] It had originally a volume of 1.7 cm³ and an extremely narrow mosaic spread of less than 0.01°, with the Curie temperature at 130 °C. Unfortunately, during the previous experiment, the crystal developed cracks which ultimately resulted in fracture. The pieces were held together mechanically for the present experiments. The resulting effective mosaic spread was anisotropic, showing in the worst projection ([110] zone) a splitting of Bragg peaks of 0.4°. Except in one instance to be mentioned later, this had little effect upon our results.

Inelastic neutron measurements were carried out at the Brookhaven High Flux Beam Reactor using a triple-axis spectrometer. Since the previous measurements on the same crystal, a significant advance has been made in the effective usage of neutrons. This is due to extremely high efficiency of pyrolytic graphite[14] used as monochromator as well as analyzer crystals. For the energy range of neutrons used for the present experiments, 45–14 meV, the use of (002) graphite reflections gave approximately 10 times the intensity compared with the deformed Ge(111) in transmission geometry.

III. SOFT OPTIC PHONONS WITH $\vec{q}$ ALONG [100]

It is clear from recent measurements on cubic[12,13] BaTiO₃ that remarkably well-defined sheets of diffuse x-ray scattering exist in planes perpendicu-
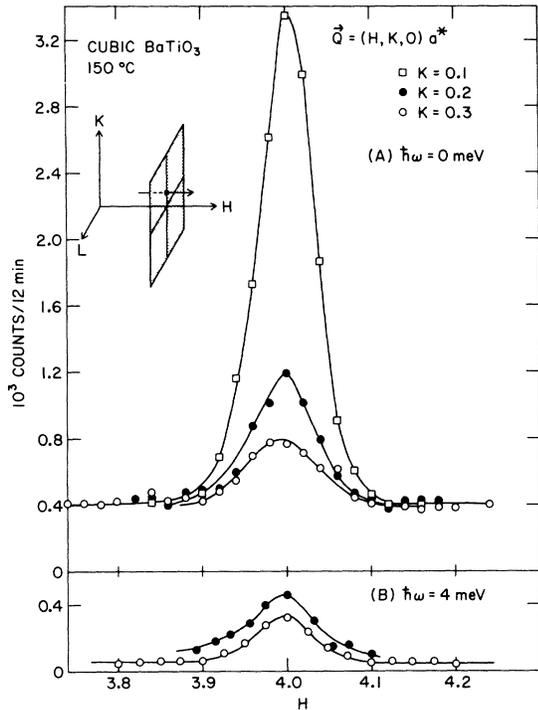
FIG. 1. Triple-axis spectrometer scans at constant energy across the sheets of diffuse scattering. The path of the scans is shown in the insert. The high background level in the elastic scan ($\hbar\omega = 0$) is due to nuclear incoherent scattering. The inelastic scans ($\hbar\omega = 4$ meV) establish the dynamical origin of the scattering. The neutron energy was 38 meV with 40-min collimation before and after the sample.

lar to [h00] reciprocal-lattice vectors and are in some way connected with the subsequent phase transformations. Our first experiments were undertaken to determine whether or not this diffuse scattering is elastic or inelastic. There has been a certain amount of controversy on this point, and x-ray measurements are not capable of providing the answer.

Figure 1 shows some of our results scanning at constant energy transfer perpendicularly through the diffuse scattering plane perpendicular to (400). Results are shown first for elastic scattering then for a neutron energy loss of 4 meV. It is readily apparent that the general features of the diffuse streaks seen by x rays exist in neutron scattering as well. It is equally apparent that the scattering is not entirely elastic. The truly elastic incoherent scattering which provides the high uniform background of Fig. 1(a) is entirely missing in Fig. 1(b), but the sheet of diffuse scattering is still clearly visible.

A more complete picture of the energy distribution of the diffuse scattering is obtained from energy scans at constant Q such as is shown in Fig.

2. When the unwanted elastic incoherent component, obtained by similar scans at a "clean" position in the reciprocal lattice, is removed, resultant profiles such as those of Fig. 3 are obtained. The very broad peak centered around $\hbar\omega = 0$ is clearly a continuation of the overdamped excitations with smaller wave vector ($q \leq 0.15a^*$, where a^* is the length of the reciprocal-lattice vector), studied in some detail by Yamada, Shirane, and Linz,[2] which displays critical behavior near the phase transformation temperature characteristic of an unstable excitation. Since the frequency components of the excitation extend to typically phonon-like frequencies, we shall for the present refer to the scattering as due to an overdamped phonon mode. We shall return to a discussion of the detailed nature of the excitation later. We must, however, point out that our experimental results differ from the earlier work of Shirane et al.[1] in that with a higher signal-to-noise ratio we were unable to identify any peaks in the scattering at $\omega \neq 0$ which we could identify with an undamped soft optic-phonon branch for any value of ζ along [ζ, 0, 0], al-
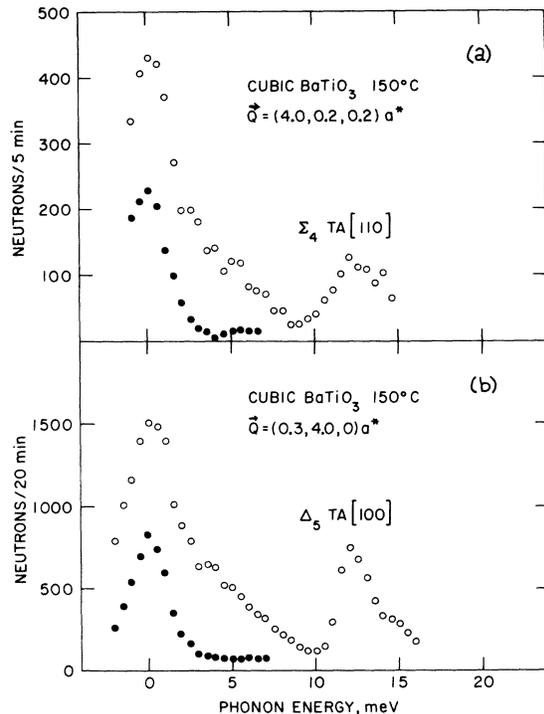
FIG. 2. Energy profile of diffuse scattering. Only the portions of the curves corresponding to phonon creation are shown. The solid points show the truly elastic nuclear incoherent background which must be subtracted to obtain the dynamical scattering profile. The peaks at 12 meV are due to TA phonons. Note the extreme similarity of profiles with q along [100] and [110]. In both cases, the phonon displacements are along a [100] direction.
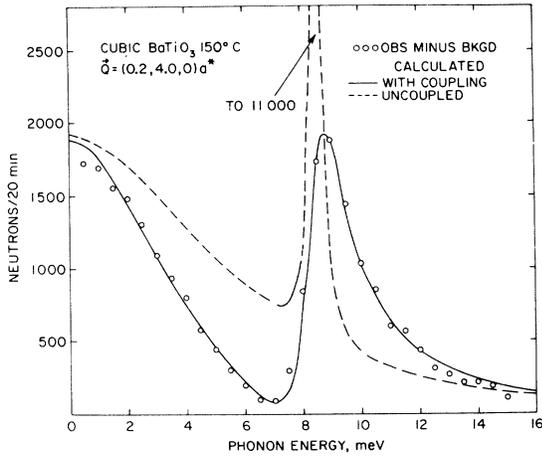
FIG. 3. Typical scattering profile such as is given in Fig. 2 with incoherent elastic background removed. The broad component centered about $\hbar\omega = 0$ is due to the over-damped soft TO mode. Both the deep minimum near $\hbar\omega = 7$ meV and the pronounced asymmetry of the TA peak are the result of anharmonic-mode interaction. The solid line is the result of the mode interference calculation described in the text.

though there is very clear evidence of *overdamped* modes over the entire region. Those sharp features which the authors noted were unusually weak, are certainly spurious and probably were caused by structure in the reflectivity of the analyzing crystal.

Notice from the extreme similarity of Figs. 2(a) and 2(b) that broad scattering peaks, attributed here to overdamped phonons, are not restricted to the [100] propagation direction but appear in the [110] direction as well. We shall see later that it is likely that a branch remains soft for *all* propagation vectors which lie in [100] planes.

Figure 3 shows in addition to the broad over - damped behavior of the soft mode, a pronounced broadening and asymmetry of the TA phonon peak. The corrections for instrumental resolution here are small so that the resulting line profile is nearly the intrinsic shape. An even more striking effect is demonstrated in Fig. 4 which compares the inelastic scattering profiles for two different values of the scattering vector $\vec{Q}$, which reduce to the same point in the first Brillouin zone (BZ), i.e., $\vec{q} = \vec{Q} - \vec{G}$ is identical in both cases. Since the phonon-frequency spectra depend upon $\vec{q}$ (not $\vec{Q}$) we should expect such related phonon groups to be identical in position and shape, and to differ only in their relative intensities one to another by virtue of the neutron-phonon coupling (the inelastic structure factors) which does depend upon $\vec{Q}$. The observed behavior, involving the disappearance of the deep minimum between peaks and the simultaneous

shift of the outer maximum by ~ 1 meV, is clearly not in agreement with these simple predictions. These and other related observations which we will describe can be understood as arising from an interference between two one-phonon states (TA and TO) with the same wave vector $\vec{q}$. Closely related interference effects involving pairs of $q \approx 0$ optic phonons have been inferred from infrared reststrahlen spectra[15] and observed more recently in Raman scattering.[16]

The scattering intensity due to creation or annihilation of a single phonon of wave vector $\vec{q}$ is proportional to a Fourier-transformed correlation function[4]

$$S_1(\omega\vec{Q}) = \sum_{jj'} F_j(\vec{Q})^* F_{j'}(\vec{Q})$$

$$\times \int_{-\infty}^{\infty} dt\, e^{-i\omega t} \langle Q_{j,-\vec{q}}(0) Q_{j',\vec{q}}(t) \rangle \cdots , \quad (1)$$

where $Q_{j\vec{q}}(t)$ is the normal coordinate of the phonon belonging to the j'th branch and $F_j(\vec{Q})$ is the inelastic structure factor. In the harmonic approximation each $Q_{j\vec{q}}$ is a statistically independent eigenstate so that the only nonvanishing terms in Eq. (1) have $j = j'$. This leads directly to the behavior predicted in the preceding paragraph. However, the presence of anharmonic interactions causes mixing of the original phonon eigenstates, and cross correlations begin to appear among normal coordinates belonging to the same irreducible represen-
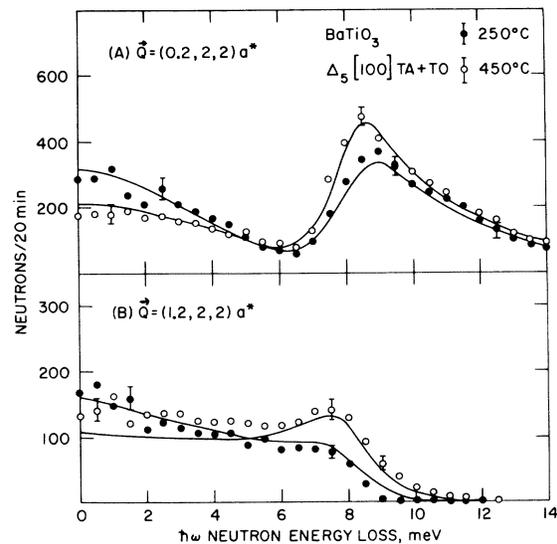
FIG. 4. Interference effects between TA and TO modes cause a shift in the apparent position and shape of the TA phonon when observed at different positions in the extended BZ. The change from a resonant to an antiresonant situation results from a change in the phase of the neutron-phonon coupling constant (dynamical strucutre factor).

TABLE I. Mode frequencies, damping and interaction parameters, and inelastic structure factors.

q (in units of a^*)	$\vec{G}$	T (°K)	$\hbar\Omega_{TO}$ (meV)	$\hbar\Gamma_{TO}$ (meV)	$\hbar\Omega_{TA}$ (meV)	$\hbar\Gamma_{TA}$ (meV)	$\hbar^2\lambda^2$ (meV)^2	F_{TO}/F_{TA}
0.2	(220)⎱ (221)⎰	450	15.0 ±3	34 ± 6	8.47 ± 0.07	1.1 ± 0.9	61.0 ± 2.9⎱ ⎰	− 2.34 ± 0.29 1.87 ± 0.14
	(220)⎱ (221)⎰	250	12.7 ±3	29 ± 5	8.47	1.1 ± 0.9	61.0 ⎱ ⎰	− 2.34 1.87
	(400)	150	9.8 ± 0.9	22 ± 2	8.50 ± 0.9	0.2 ± 0.1	44.0 ± 5.2	− 2.16 ± 0.4
0.3	(400)	150	13.9 ± 0.5	33.2 ± 1	11.7 ± 0.2	0.3 ± 0.2	80.0 ± 1	− 2.47 ± 0.15

tation of the space group of the lattice. As an alternative more intuitive description, one may consider the one-phonon excitations as intermediate states which decay into more complicated multiphonon final states. But inasmuch as two or more one-phonon states feed the same final states, one observes a true quantum-mechanical interference between two competing scattering channels. The result of the off-diagonal interference terms in Eq. (1) is to render nonadditive the intensities of the wings of the one-phonon scattering profiles of such coupled phonon pairs, and the profiles thus take on an asymmetric appearance. The fact that behavior of this kind is to be expected in neutron-scattering experiments on anharmonic crystals has been discussed by several authors, most notably by Cowley,[17] but has not been observed. Note that neutron scattering offers the additional possibility of altering or even reversing the sign of the interference by making observations at different but equivalent values of $\vec{Q}$, thereby changing the neutron-phonon coupling constants $F_{j\vec{q}}(\vec{Q})$. We will show that this accounts for the changes noted in Fig. 4.

In order to demonstrate the degree of quantitative agreement of these ideas with our observations, we evaluate in the Appendix an explicit form for Eq. (1) for a single pair of interacting modes. The result is

$$\frac{d^2\sigma}{d\Omega d\omega} \propto \frac{kT}{A^2 + \omega^2 B^2} \{[(\Omega_2^2 - \omega^2)B - \Gamma_2 A]F_1^2$$

$$+ 2\lambda B F_1 F_2 + [(\Omega_1^2 - \omega^2)B - \Gamma_1 A]F_2^2\} \cdots , \quad (2)$$

where

$$A = (\Omega_1^2 - \omega^2)(\Omega_2^2 - \omega^2) - \omega^2\Gamma_1\Gamma_2 - \lambda^2 \cdots ,$$

$$B = \Gamma_1(\Omega_2^2 - \omega^2) + \Gamma_2(\Omega_1^2 - \omega^2) \cdots , \quad (3)$$

and Ω_i and Γ_i represent the renormalized (quasiharmonic) phonon-frequency and mode-damping parameters, respectively.

Analysis of the observed scattering cross sections was carried out by least-squares adjustment of the parameters in Eq. (2). Some of the results are shown in Table I, and the quality of the resulting fits, shown in Figs. 3 and 4, is quite satisfying. The parameters themselves, particularly Ω_{TO} and

Γ_{TO} are of interest, since they offer the best estimate, to date, of the projected behavior of the soft mode free from damping and mode interaction effects. (In this analysis, we neglected corrections due to instrumental resolution and mosaic spread of the crystal because, in general, the observed scattering cross section is very much broader than that of the resolution function. There is one parameter, however, namely, Γ_{TA} which could be substantially affected by a more careful consideration of the crystal mosaic spread. It seems likely, in fact, that the difference between Γ_{TA} reported at 150 °C and at higher temperatures is principally not a temperature effect at all but reflects the different mosaic structures for the two different scattering geometries in which the data were taken. Hence the large error limits.) It is, for example, presumably the quasiharmonic frequency Ω_{TO} which
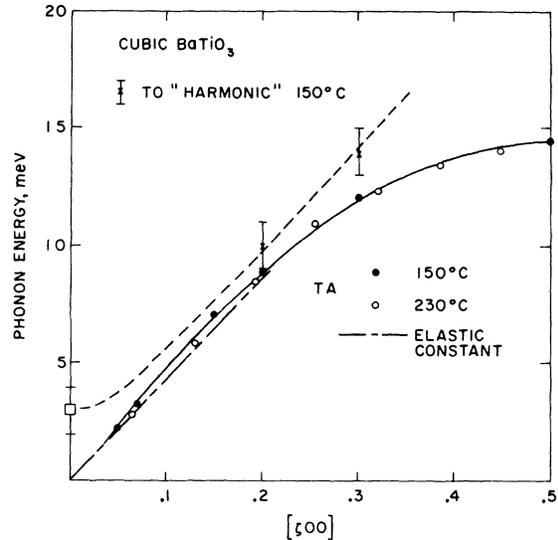
FIG. 5. Phonon-dispersion curve for the TA and soft TO branches along [100]. For the acoustic branch (solid line) the observed mode frequencies are given. For the optic branch the quasiharmonic frequencies deduced from optical (□) or neutron-scattering (✗) experiments are given. The dotted line is of the form $(\hbar\omega)^2 = (\hbar\omega_0)^2 + \Lambda q^2$.

must be compared with any lattice-dynamical calculations which ignore dissipative effects. The estimated behavior of Ω_{TO} is indicated in Fig. 5. Notice that the mode overdamping condition Γ_{TO} > $2\Omega_{TO}$ is weakly satisfied at all temperatures and $\vec{q}$ values listed in Table I. In fact, we find the empirical relation $\Gamma_{TO}/\Omega_{TO} = 2.3$ holds rather well over the range of $\vec{q}$ and temperatures investigated. This can be compared with the value $\Gamma/\Omega \simeq 4{-}6$ at $q \simeq 0$ deduced from optical measurements in the same temperature region[8] and $\Gamma/\Omega \simeq 9$ at $q = 0.08a^*$.[2] Correction for mode-coupling effects discussed here will lower this latter figure somewhat. From estimates of the soft-mode eigenvector, derived from the tetragonal structure, we may calculate in the limit $q \to 0$, $F_{TO}(400)/F_{TA}(400) = F_{TO}(220)/F_{TA}(220) = -1.7$ and $F_{TO}(221)/F_{TA}(221) = 4.0$. Since the values given in Table I are deduced for finite q, the qualitative agreement is satisfying. This analysis gives the first experimental determination of the relative polarity of phonon structure factors.

A few remarks are in order concerning the relationship of the anharmonic mode coupling discussed here with another source of abnormal acoustic dispersion in materials with soft optic modes discussed in a previous paper.[18] In this latter case, the familiar anticrossing behavior of two modes of the same symmetry type was formulated as a "mode-coupling" problem. This was done by choosing $q = 0$ eigenstates as basis states for the dynamical matrix at small but finite q. Normal *harmonic forces* provide the coupling of these "bare" (i.e., $q = 0$) modes at finite q. The only important anharmonicity in this problem is that diagonal part which provides a temperature-dependent $q = 0$ optical-mode frequency. Although this proved to be a convenient and physically satisfying description, it is "fictitious" in the sense that the new coupled modes are independent normal modes of the finite q dynamical matrix in the quasiharmonic approximation. However, after this essentially harmonic coupling of $q = 0$ basis states has been carried out there may remain anharmonic forces coupling the two harmonic modes together through multiphonon excitations. In the limit of small damping, the anharmonic coupling simply produces an additional repulsion between the two levels. The unique interference aspects observed in the present experiments become important only if at least one of the interacting modes becomes sufficiently broadened to allow appreciable overlap of the spectral response of the two excitations.

IV. ANISOTROPIC DISPERSION AND DESCRIPTION OF SOFT OPTIC MODES NEAR $\vec{q} = 0$

In contrast to the very soft and heavily damped behavior of the phonons which we have just dis-

cussed, most other phonons in the lowest TO branches have energies which increase rapidly with q to normal values. The dispersion is in fact so large that satisfactory intensity peaks could not be detected by the usual constant Q scanning technique. The behavior was better studied by constant E scanning, as shown by the typical intensity profiles of Fig. 6. The relatively weak signals are a direct consequence of the steep dispersion which results in a small density of modes within the experimental resolution function. In such scans instrumental resolution effects can also result in broadened peaks shifted somewhat from that of the true excitations. The corrections required for such instrumental shifts can be calculated numerically, convoluting the instrumental resolution function with the dispersion surface, provided that a suitable analytical form for the dispersion surface is known. The present data have been corrected in this manner and in the process simple approximate analytical expressions for $\omega^2(j\vec{q})$ near $q = 0$ were developed. These expressions, first of all, form a convenient representation of our experimental results, and second, may be useful in discussing any of the many physical properties which depend upon the soft-phonon density of states. A short discussion of this topic is therefore of interest.

There are in fact two soft TO branches near $\vec{q} = 0$. The branches coalesce along the high-symmetry [100] and [111] directions but are, in general, distinct for other directions of $\vec{q}$. In the [110] direction one branch is polarized along a cube-face
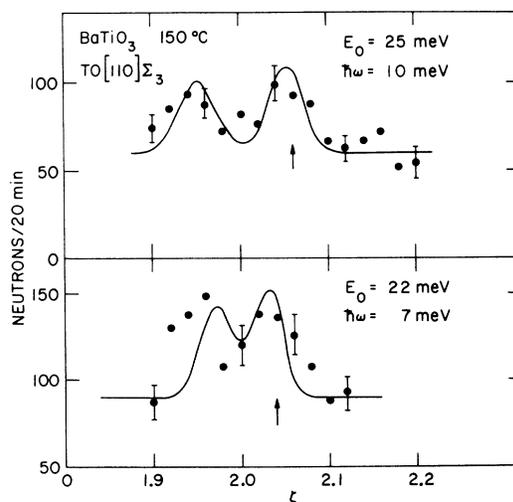
FIG. 6. Constant energy scans taken in a $[\zeta\zeta 0]$ path about the reciprocal-lattice point $(2\bar{2}0)$ cut both sides of the TO phonon branch which rises sharply from its minimum at the reciprocal-lattice point. Conventional energy scans at constant Q yield very broad peaks indistinguishable from the background in these instances.

diagonal (T_1 or Σ_3), the other is polarized along a cube edge (T_2 or Σ_4), and we shall consequently refer to them as branches 1 and 2, respectively. Technically, the critical point at $q = 0$ is an example of a fluted critical point,[19] i. e., although $\omega^2(j\vec{q})$ cannot be represented in a simple Taylor expansion about $q = 0$, it can be expanded in the form

$$\hbar^2\omega^2(j\vec{q}) = \hbar^2\omega^2(0) + \Lambda_j(\hat{q}) \cdot |\vec{q}|^2 + Oq^4 + \cdots , \quad (4)$$

or, in other words, Λ_j may depend upon the direction $\hat{q} \equiv \vec{q}/|\vec{q}|$ of q.

Whereas $\omega^2(0)$ exhibits a strong temperature dependence, Λ should be nearly temperature independent. Exploiting the symmetry properties of cubic BaTiO$_3$, $\Lambda(\hat{q})$ was approximated in terms of the lowest-order cubic harmonics. By determining the $\Lambda_j(\hat{q})$ coefficients from the experimentally measured values of Λ along the three principal directions, we find that

$$\Lambda_j(\hat{q}) = [2\Lambda_j(110) - \Lambda(110)] - 2[\Lambda_j(110) - \Lambda(100)]$$
$$\times (\hat{q}_x^4 + \hat{q}_y^4 + \hat{q}_z^4) - [36\Lambda_j(110) - 9\Lambda(100) - 27\Lambda(111)]$$
$$\times (\hat{q}_x^2\hat{q}_y^2\hat{q}_z^2) + \cdots , \quad (5)$$

where ($\hat{q}_x, \hat{q}_y, \hat{q}_z$) are components of the unit vector $\hat{q}$. See also Fig. 7.

Computed intensity profiles based upon a convolution of frequencies based upon Eqs. (4) and (5) with the known instrumental resolution were compared with the experimentally observed profiles. For this purpose the dynamical structure factors were assumed to be independent of the direction of $\vec{q}$. The parameters were then adjusted for self-consistency. The parameters finally arrived at in this way are

$$\hbar\omega_0 = (3 \pm 1)\,\text{meV} \quad \text{at} \quad T = 150\,°\text{C} \quad (\text{Ref. 20}),$$

$$\Lambda_1(110) = \Lambda(111) = (4750 \pm 300)\,(\text{meV Å})^2 ,$$

$$\Lambda(100) = (972 \pm 50)\,(\text{meV Å})^2 ,$$

$$\Lambda_2(110) \approx \Lambda(100) .$$

The values of $\Lambda(100)$ and $\Lambda_2(110)$ come from the analysis of the coupled-mode problem discussed in Sec. III. An example of the fit of the resultant calculation to the observed intensity profile in a "hard" direction is shown in Fig. 6. In contrast to the situation described in Sec. III, the linewidth is fitted in a reasonably satisfactory way without invoking additional intrinsic phonon lifetime broadening.

Strong anisotropy in the soft branches of BaTiO$_3$ has been predicted by Hüller[21] to arise from the harmonic contribution of polarization-enhanced dipolar interactions. While the present results do in fact confirm his predictions to a remarkable extent, it should be pointed out that the soft-mode

dispersion in PbTiO$_3$, with seemingly similar dipolar forces, is much more nearly isotropic.[22]

Finally, we have extended our measurements to large q to complete the dispersion of the lowest-energy branches along the principal symmetry directions. Data have been previously reported for the [100] direction and are in good agreement with Fig. 5 with the exception noted previously concerning the spurious sharp peak attributed to the soft TO branch. In view of the extreme breadth of the true soft excitation, the only meaningful single frequencies for the TO branch which can be given are the estimates for the quasiharmonic frequencies shown in Fig. 5. For the remaining propagation directions, the data are summarized in Figs. 8 and 9. Also, not shown in Fig. 8, we have determined the frequency of the triply degenerate Γ_{25} modes at the BZ center,[23] which are neither infrared or Raman active. The mode assignment was made by comparison of calculated and observed structure factors at various reciprocal-lattice points. The frequency was found to be (39 ± 2) meV.
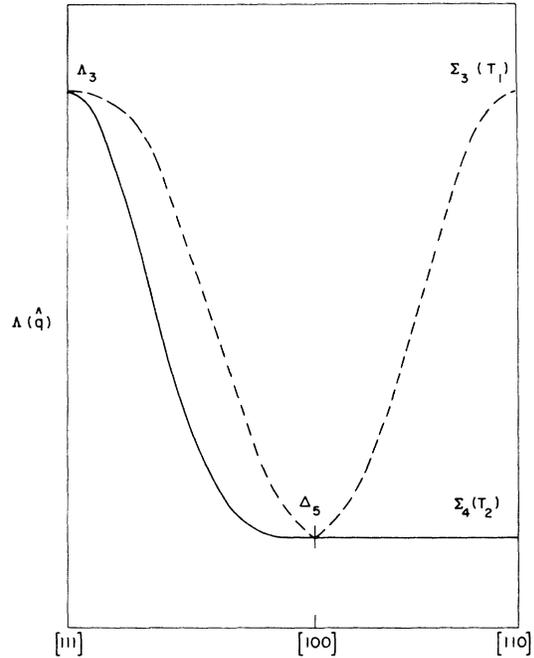
FIG. 7. Anisotropy of the soft TO branches near $q = 0$ according to Eq. (5). The abscissa is the angular orientation of $\vec{q}$ along arcs connecting the major symmetry axes. The quasiharmonic phonon frequencies are given as a function of the direction $\hat{q}$ of the wave vector, $(\hbar\omega)^2 = (\hbar\omega_0)^2 + \Lambda(\hat{q})q^2$. Note that within this approximation the TO branch is soft for all wave vectors lying in (100) planes. This gives rise to strong one-dimensional dynamical correlations and accounts for the sheets of diffuse scattering observed with x rays.

V. CONCLUSIONS

The data of the preceding sections establish both the extreme anisotropy of the low-frequency optical-phonon dispersion and the overdamped inelastic character of the pronounced diffuse scattering sheets in cubic $BaTiO_3$ observed by x rays. Both of these results serve to clarify certain aspects of the order-disorder model introduced by Comes et al.[13] to explain their x-ray results. They consider cubic $BaTiO_3$ to be intrinsically disordered, being the result of chains of displaced atoms, the chains lying along the principal cubic axes. However, as Hüller[24] has shown in detail, an anisotropic distribution of optic-phonon frequencies such as is shown in Fig. 7 also leads to sheets of diffuse scattering and to atomic displacements strongly correlated along $\langle 100 \rangle$ directions but in an instantaneous, not a static sense. If we add the reasonable possibility of the lowest-frequency optic modes becoming overdamped, this picture of dynamical phononlike correlations seems to fit our observations in all details. It is therefore our opinion that it is somewhat misleading to consider cubic $BaTiO_3$ as a disordered phase. For it is correct only in a dynamical sense, and, of course, all crystal lattices are dynamically disordered by vibrational motion.

Having said this, we must go on to admit that it is becoming increasingly clear that the terms "displacive" and "order-disorder" really describe only limiting behavior and that physical systems may be distributed more or less continuously between these extremes. Suppose, for example, we consider the form of the collective potential experienced by an optic-lattice distortion of a given wave

FIG. 9. Typical energy profile of an inelastically scattered neutron group in $BaTiO_3$, demonstrating the general quality of the phonons which are not affected by abnormal damping. The solid line is the shape predicted as the result of finite resolution for undamped phonons.

vector in $BaTiO_3$. Has it but a single minimum, or multiple minima for some values of $\vec{q}$ (e. g., along $\langle 100 \rangle$) but not for others? This is quite logical and a conceptually important question for which there are no answers at present. In defense of the phonon picture, we do find that, even insofar as the details of the anharmonic coupling of modes is concerned, the behavior of the soft branch seems to be adequately described in terms of the simplest sort of anharmonic phonon theory. Yet it is known from investigations of the solidified gases that very anharmonic potentials can, nevertheless, give rise to excitations which upon observation behave very much like normal harmonic phonons.

ACKNOWLEDGMENTS

APPENDIX: TWO-PHONON INTERFERENCE

Several authors[17] have given implicit expressions for the indirect coupling of single-phonon excitations through the multiphonon continuum by Green's-function techniques. We sketch here an explicit formulation for two interacting phonons based upon the equation-of-motion method of Lax[25] which

FIG. 8. Experimentally determined low-lying phonon-dispersion curves for cubic $BaTiO_3$ along the principal symmetry directions. With the exceptions noted on the figure the lines have no theoretical significance.

closely parallels a simple classical description.[15]

The Fourier-transformed correlation function is first rewritten, making use of one form of fluctuation-dissipation theorem,

$$\int_{-\infty}^{\infty} dt\, e^{i\omega t} \langle A(0)B(t)\rangle = 2\hbar[n(\omega)+1]\,\mathrm{Im}\chi_{BA}(\omega) ,$$

(A1)

where $\chi_{BA}(\omega)$ defines the linear response $\langle B(t)\rangle$ $=\chi_{BA}f_A^0 e^{i\omega t}$ to an applied forcing potential V $=Af_A^0 e^{i\omega t}$. The most general motion of a normal phonon coordinate (limited to the required linear response) is of the form

$$\langle \ddot{Q}_\mu(t)\rangle = -\omega_\mu^2 \langle Q_\mu(t)\rangle - \sum_{\mu'}\int_0^\infty d\tau\, B_{\mu\mu'}(\tau)$$

$$\times \langle Q_{\mu'}(t-\tau)\rangle - f_{-\mu}^0 e^{i\omega t} , \quad \text{(A2)}$$

where $\mu \equiv (j,\vec{q})$ and $-\mu \equiv (j,-\vec{q})$, ω_μ is the harmonic frequency. The kernel $B_{\mu\mu'}(\tau)$ specifies the coupling of two modes via fluctuations in the reservoir, which in this case, are the remaining modes. Using lower-case letters for Fourier transforms we find

$$\sum_{\mu'}[(\omega_\mu^2 - \omega^2)\delta_{\mu\mu'} + b_{\mu\mu'}(\omega)]\langle q_{\mu'}(\omega)\rangle = -f_{-\mu}^0 , \quad \text{(A3)}$$

which for the case of two coupled modes ($\mu = 1, 2$) leads to the following expressions for the generalized susceptibilities $\langle q_\mu(\omega)\rangle \equiv \chi_{\mu\mu'}f_{-\mu'}^0$:

$$\chi_{11} = \chi_1^0(1 - b_{12}b_{21}\chi_1^0\chi_2^0)^{-1} ,$$

$$\chi_{12} = b_{12}\chi_1^0\chi_2^0(1 - b_{12}b_{21}\chi_1^0\chi_2^0)^{-1} ,$$

(A4)

where

$$\chi_\mu^0 \equiv -[(\Omega_\mu^2 - \omega^2) + i\omega\Gamma_\mu]^{-1} ,$$

$$\Omega_\mu^2 \equiv \omega_\mu^2 + \mathrm{Re}\, b_{\mu\mu}; \quad \omega\Gamma_\mu \equiv \mathrm{Im}\, b_{\mu\mu} ,$$

$$b_{\mu\mu'}(\omega) \equiv \int_0^\infty d\tau\, e^{-i\omega\tau}B_{\mu\mu'}(\tau) .$$

(A5)

χ_{22} and χ_{21} are obtained from (A4) by permutation of indices.

While the anharmonic self-energies $b_{\mu\mu'}(\omega)$ can, in principle, be evaluated by knowledge of the anharmonic lattice potential, it is sufficient for the present purpose to use the low-frequency asymptotic expressions

$$\mathrm{Re}\, b_{\mu\mu'}(\omega) = b_{\mu\mu'}^0 + O(\omega^2) + \cdots ,$$

$$\mathrm{Im}\, b_{\mu\mu'}(\omega) = \omega[\Gamma_{\mu\mu'}^0 + O(\omega^2) + \cdots] ,$$

(A6)

which follow from the fact that Reb and Imb are, respectively, even and odd functions of ω. In particular, we expect that Im$b_{12} \ll$ Reb_{12} at low frequencies and thus we may approximately set b_{12} $= b_{21} = -\lambda$, a real constant. Combining these relations with the high-temperature approximation $n(\omega) = kT/\hbar\omega > 1$ we arrive finally at the explicit expression given in Eq. (2).

[1]G. Shirane, B. C. Frazer, V. J. Minkiewicz, J. A. Leake, and A. Linz, Phys. Rev. Letters 19, 234 (1967).

[2]Y. Yamada, G. Shirane, and A. Linz, Phys. Rev. 177, 848 (1969). We take this opportunity to correct two numerical errors in this paper. On p. 852, $A = 0.043$ $\times 10^{-2}$ Å^{-2} deg^{-1}, and on p. 854, $\hbar\omega \cong 3.4 \times 2 = 6.8$ meV.

[3]G. Shirane, J. D. Axe, J. Harada, and A. Linz, Phys. Rev. B 2, 3651 (1970).

[4]See, for example, the recent review by W. Cochran, Advan. Phys. 18, 157 (1969).

[5]W. Cochran, Advan. Phys. 9, 387 (1960).

[6]J. M. Ballantyne, Phys. Rev. 126, 1710 (1962).

[7]W. G. Spitzer, R. G. Miller, D. A. Kleinman, and L. E. Howarth, Phys. Rev. 126, 1710 (1962).

[8]A. S. Barker, Phys. Rev. 145, 391 (1966).

[9]M. DiDomenico, Jr., S. P. S. Porto, and S. H. Wemple, Phys. Rev. Letters 19, 855 (1967).

[10]J. L. Parsons and L. Rimai, Solid State Commun. 5, 423 (1967).

[11]A. Pinczuk, W. Taylor, E. Burstein, and I. Lefkowitz, Solid State Commun. 5, 429 (1967).

[12]J. Harada and G. Honjo, J. Phys. Soc. Japan 22, 45 (1967).

[13]R. Comès, M. Lambert, and A. Guinier, Solid State Commun. 6, 715 (1968); 7, 305 (1969).

[14]T. Riste and K. Otnes, Nucl. Instr. Methods 75, 197 (1969).

[15]A. S. Barker, Jr. and J. J. Hopfield, Phys. Rev. 135, A1732 (1964).

[16]D. L. Rousseau and S. P. S. Porto, Phys. Rev. Letters 20, 1354 (1968); E. Burstein, S. Ushioda, A. Pinczuk, and J. F. Scott, in Light Scattering Spectra of Solids, edited by G. Wright (Springer-Verlag, New York, 1969), p. 43.

[17]R. A. Cowley, Advan. Phys. 12, 421 (1963), and references therein.

[18]J. D. Axe, J. Harada, and G. Shirane, Phys. Rev. B 1, 1227 (1970).

[19]J. C. Phillips, Phys. Rev. 104, 1263 (1956).

[20]Taken from the analysis of infrared reflectivity measurements given in Ref. 8.

[21]A. Hüller, Z. Physik 220, 145 (1969).

[22]G. Shirane, J. D. Axe, J. Harada, and J. P. Remeika, Phys. Rev. B 2, 155 (1970).

[23]We use throughout this paper a group-theoretical notation consistent with that introduced in discussing SrTiO$_3$ by R. A. Cowley [Phys. Rev. 134, A981 (1964)].

[24]A. Hüller, Solid State Commun. 7, 589 (1969).

[25]M. Lax, J. Chem. Phys. Solids 25, 487 (1964).

FIG. 1. Triple-axis spectrometer scans at constant energy across the sheets of diffuse scattering. The path of the scans is shown in the insert. The high background level in the elastic scan ($\hbar\omega = 0$) is due to nuclear incoherent scattering. The inelastic scans ($\hbar\omega = 4$ meV) establish the dynamical origin of the scattering. The neutron energy was 38 meV with 40-min collimation before and after the sample.